20th Australasian Fluid Mechanics Conference
Perth, Australia
5-8 December 2016

Numerical simulation of vortex-induced vibration of two long flexible circular cylinders in tandem

Hao Wu[1,2], Lin Lu[1], Ming Zhao[2] and Song Yan[1]

[1] State Key Laboratory of Coastal and Offshore Engineering
Dalian University of Technology, Dalian, 116024, China

[2] School of Computing, Engineering and Mathematics
Western Sydney University, Penrith, NSW 2751, Australia

Abstract

A quasi three-dimensional numerical model is developed to study vortex-induced vibration (VIV) of two tandem flexible circular cylinders. In this model, the whole cylinder is divided into many sections along its length. The hydrodynamics of each section are represented by the solution of the two-dimensional Navier-Stokes equations. The dynamic response of the flexible cylinder is predicted by the solution of the three-dimensional equations of motion of a tensioned vertical cylinder. Simulations of two identical cylinders are carried out with a same mass ratio of 2.453 and a large aspect ratio of 3691. The centre-to-centre distance between two tandem cylinders is 5*D*. A low Reynolds number of 200 is used in the simulations, and the reduced velocity based on the fundamental natural frequency is 32.1. The numerical results show that the sixth mode vibration is excited on the upstream cylinder and its dynamic response is very similar to that of the isolated cylinder. However, due to the effect of wake interference, the response of the downstream cylinder is quite different from that of the upstream cylinder. It is mainly controlled by the third order mode although multi-mode vibration is involved. The highly irregular vortex shedding pattern of the downstream cylinder is distinct to the regular 2S vortex shedding mode of the upstream cylinder.

Introduction

Vortex-induced vibration (VIV) of circular cylinders has been studied extensively because of its significance in engineering applications. The VIV of two cylinders in close proximity has attracted considerable attention. Sumner [8] and Bearman [2] reviewed the research on the flow interference of two cylinders. So far, the majority of numerical studies for the VIV of two cylinders are two-dimensional (2D) simulations of elastically supported cylinders, such as Mittal and Kumar [6] and Zhao [11]. It is still a great challenge to carry out fully three-dimensional (3D) simulations of VIV of flexible cylinders owing to its huge computational efforts. Fully 3D numerical models are usually applied to elastically supported, short rigid cylinders (Carmo et al. [3] and Assi et al. [1]). A practical approach to simulate VIV of long, flexible cylinders is to use the quasi 3D models which perform 2D CFD solutions on multiple sections along the cylinder span, instead of fully 3D CFD solutions, and thus improve the computational efficiency significantly. These models have been applied in the numerical studies of VIV of an isolated flexible cylinder, e.g. Schulz et al. [7], Willden et al. [9], Yamamoto et al. [10], and proved to be successful in comparison with experimental results. However, the numerical studies on multiple flexible cylinders in proximity remains scarce, which is the main concern of this study.

In the present work, VIV of two tandem flexible cylinders in proximity is studied numerically by using the proposed quasi 3D model. Numerical results include the dynamic response, fluid force and vortex shedding pattern are presented. The results of an isolated flexible cylinder are also provided for comparison.

Numerical Method

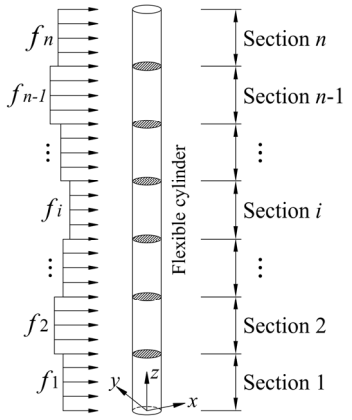

Figure 1. Defining sketch of fluid-structure coupling model

As shown in Figure 1, the cylinder span is divided into multiple sections, and each section is represented by a 2D CFD strip at the centre of the section, where n is the number of sections. The fluid force on each section is assumed to be distributed evenly. f_i denotes the fluid force per unit length on the section i, which is calculated by solving the 2D incompressible Navier-Stokes (NS) equations. The Arbitrary Lagrangian Eulerian (ALE) method is applied to deal with the moving boundary of the vibrating cylinder. The velocity u, the coordinate x, the time t and the pressure p are normalized by the inlet flow velocity U, the diameter of cylinder D and fluid density ρ as $u = \tilde{u}/U$, $x = \tilde{x}/D$, $t = \tilde{t}U/D$, $p = \tilde{p}/\rho U^2$, where the tilde denotes the dimensional parameters. The nondimensional ALE formulation for the NS equations are expressed as

$$\frac{\partial u_i}{\partial x_i} = 0$$
$$\frac{\partial u_i}{\partial t} + (u_j - u_j^m)\frac{\partial u_i}{\partial x_j} = -\frac{\partial p}{\partial x_i} + \frac{1}{\mathrm{Re}}\frac{\partial^2 u_i}{\partial x_j^2} \quad (1)$$

where $i, j = 1, 2$ denotes the Cartesian coordinates components in the in-line and the cross-flow directions of the flow, respectively. u_i is the fluid velocity component in the x_i-direction. u_j^m is the velocity of a mesh node and Re is the Reynolds number.

Equation (1) is solved by a three-step finite element method. The details of this method can be found in Tang et al. [5].

The dynamic response of the cylinder is calculated by solving the equations of motion. In this study, the vibration of the cylinder is

restricted in the cross flow direction. Assuming that the cylinder is elastic and homogeneous, the equations of motion of a tensioned vertical cylinder are expressed as

$$EI\frac{\partial^4 Y}{\partial z^4}-\frac{\partial}{\partial z}\left(T\frac{\partial Y}{\partial z}\right)+m\frac{\partial^2 Y}{\partial t^2}+c\frac{\partial Y}{\partial t}=F_y \qquad (2)$$
$$m\frac{\partial^2 Z}{\partial t^2}-EA\frac{\partial^2 Z}{\partial z^2}=0$$

where Y is the displacement of the cylinder in the cross flow direction, z is the Cartesian coordinate in the axial direction of the cylinder, Z is the displacement of the cylinder in the z-direction, EI is the flexural rigidity, EA is the tensile stiffness, m is the mass per unit length, T is the tension, c is the structural damping and F_y is the lift force generated by the fluid flow.

By applying the Galerkin finite element method, equation (2) can be converted to the matrix equation

$$\mathbf{M}\ddot{\mathbf{d}}+\mathbf{C}\dot{\mathbf{d}}+[\mathbf{K}_E+\mathbf{K}_G(\mathbf{d})]\mathbf{d}=\mathbf{F} \qquad (3)$$

where $\mathbf{M}$, $\mathbf{C}$, $\mathbf{K}_E$ and $\mathbf{K}_G$ are the mass matrix, the damping matrix, the elastic stiffness matrix and the geometric stiffness matrix, respectively. $\mathbf{F}$ is the load vector and $\mathbf{d}$ is the displacement vector. Equation (3) is solved by the Newmark scheme with integral parameters of α=0.25, δ=0.50.

A weak-coupling strategy is adopted to deal with the flow-structure coupling. At each computational time step, the fluid forces and the structural response are calculated alternately. Because the 2D CFD simulation on each strip is independent, it is easy to implement the parallel computing. A parallel program based on master-slave pattern using the OpenMP interface is developed in this study.

For each CFD strip, a rectangular computational domain with a length of 85D (flow direction) and a width of 50D (cross flow direction) is discretized into quadrilateral finite elements. The center of the upstream cylinder is located 25D from the inlet boundary, with equal distance to the lateral boundaries. Numerical simulations for a single isolated cylinder are also conducted for the purpose of comparison. The computational mesh near the two tandem cylinders is shown in Figure 2.

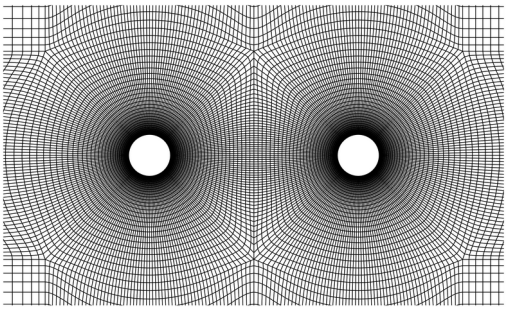

Figure 2. Computational mesh near the tandem cylinders

Numerical Results

Numerical simulations are carried out on the VIV of two identical circular cylinders in tandem arrangement and an isolated cylinder. The length to diameter ratio of the cylinder is L/D = 3691. The center-to-center distance between the two cylinders is 5D. The mass ratio m^* (the ratio of the mass of the cylinder to displaced fluid) is 2.45. The damping ratio ζ is 0.02. This work focus on testing the effectiveness of the proposed quasi 3D model. Simulations are performed to a low Reynolds number of 200 in the 2D laminar flow regime. It was known that the Strouhal number, defined as St = f_sD/U, is close to 0.2 for Re = 200 (Lienhard [4]), where f_s is the vortex shedding frequency. Furthermore, the nondimensional natural frequency is defined as f_nD/U, where f_n is the n-th mode natural frequency of the cylinder. In order to excite the sixth mode vibration of the cylinder, the elastic properties of the cylinder were chosen in a way that f_6D/U = 0.187, i.e. the vortex shedding frequency is slightly greater than the sixth natural frequency. The nondimensional natural frequencies of the first to eighth mode of the cylinder are listed in Table 1, which are calculated by a superposition method using the present structural model. Accordingly, the reduced velocity based on the fundamental natural frequency is $U_r = U/f_1D$ = 32.1.

Mode	1	2	3	4	5	6	7	8
f_nD/U	0.031	0.062	0.093	0.125	0.156	0.187	0.219	0.251

Table 1. Nondimensional natural frequency of the cylinder

Fifty CFD strips are allocated along the cylinder span with equal spacing. The cylinder is discretized into 500 finite elements for solving the equations of motion. The nondimensional flow velocity at the inlet boundary is 1. The gradient of the flow velocity in the normal direction and the relative pressure are zero at the outflow boundary. The gradient of the flow velocity and the pressure in the cross-flow direction are zero at the lateral boundaries. The flow velocity on the surface of the cylinder is equal to the movement speed of the cylinder. The constrain of the bottom end of the cylinder is fixed-hinged and that of the top end of the cylinder is sliding-hinged. That means the top end of the cylinder is capable of axial motion.

Figure 3 shows the envelope and standard deviation of the displacement in the cross flow direction for the isolated cylinder and the tandem cylinders. It is observed from Figure 3(a) that the vibration of the isolated cylinder is symmetric with respect to its static position. The curve shapes of the Figure 3(a) and (b) indicate that the vibration mode of the isolated cylinder is sixth order, which is consistent with previous prediction. The points of the minimum and maximum vibrations on the curve shape are referred to as nodes and antinodes, respectively. The constant locations of the six nodes and six antinodes suggest a standing wave vibration of the isolated cylinder. The displacements of the antinodes near the two cylinder ends are greater than the displacement near the middle position, and the maximum displacement appears close to the bottom end. This is mainly because of the gravity and the sliding-hinged constrain on the top end. The maximum displacement of the isolated cylinder is 0.72D, appearing at the bottom antinode. It should be noted that the displacements of the nodes are not zero, which is resulted from the low-order modes involved in the vibration of the isolated cylinder.

For the tandem cylinders, it can be seen from Figure 3(c) that the vibration shape of the upstream cylinder is similar to that of the isolated cylinder, which is also dominated by the sixth order mode. Due to the interference of the downstream cylinder, the displacements of antinodes on the negative side are slightly greater than those on the positive side, which leads to that the mean position of the upstream cylinder deviates from the static position. The maximum displacement of the upstream cylinder is 0.80D, which is slightly greater than that of the isolated cylinder. The displacements of the nodes of the upstream cylinder are much greater than those of the isolated cylinder, suggesting significant multi-modes vibration. It seems that the present spacing distance of 5D gives rise to a weak influence on the upstream cylinder from the downstream cylinder. However, the wake interference has more profound effect on the cylinder downstream. The dynamic response of the downstream cylinder is quite different from that of the upstream cylinder. It is observed from Figure 3(d) that the vibration of the downstream cylinder is primarily dominated by the third order mode, whereas the envelope of displacement shown in Figure 3(c) indicates the participation of the sixth order mode. Figure 3(c) also shows that

the vibration of the downstream cylinder is no longer symmetric. The vibration shape of the downstream cylinder is irregular, with much greater amplitude than that of the upstream cylinder. However, Figure 3(d) shows that the standard deviation of the antinode displacements of the downstream cylinder is smaller or close to those of the upstream cylinder. This means that considerable deviation of the mean position from the static position and the multi-modes vibration are involved. The maximum displacement of the downstream cylinder is 1.05*D*.

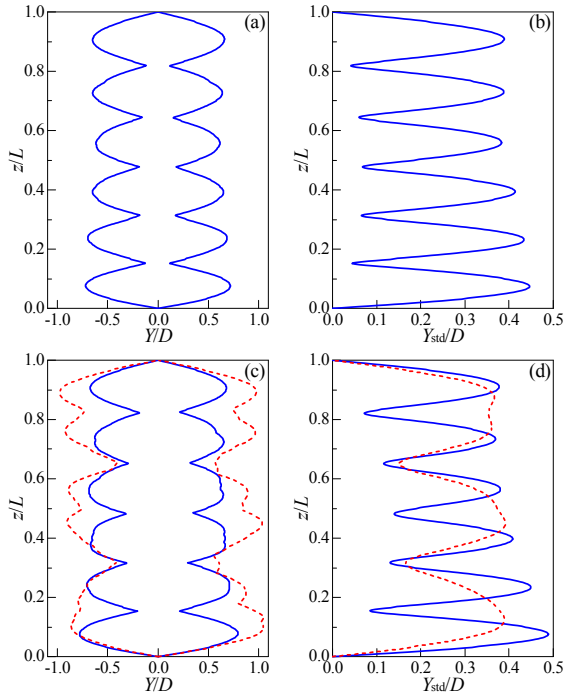

Figure 3. Envelope and standard deviation of the displacement in the cross flow direction for the isolated cylinder (a, b) and the tandem cylinders (c, d). Solid line: upstream cylinder; Dash line: downstream cylinder.

Figure 4 shows the mean and standard deviation of the drag coefficient and lift coefficient for the isolated cylinder and the tandem cylinders. It can be seen from Figure 4(a, b, c) that for the isolated cylinder, the distribution tendencies of $C_{D\text{mean}}$ and $C_{D\text{std}}$ are consistent with Y_{std}, while that of $C_{L\text{std}}$ is contrary to Y_{std}. This means that the greater drag amplitudes appear at the antinodes with a large displacement, while the greater lift amplitudes appear at the nodes with a small displacement. The maximum $C_{D\text{mean}}$, $C_{D\text{std}}$ and $C_{L\text{std}}$ of the isolated cylinder is 2.13, 0.63 and 1.05, respectively. For the tandem cylinders, it is observed from Figure 4(d, e, f) that the variation trend and the amplitude of the fluid force of the upstream cylinder are similar to those of the isolated cylinder. This explains why their dynamic responses are similar. The maximum $C_{D\text{mean}}$, $C_{D\text{std}}$ and $C_{L\text{std}}$ of the upstream riser is 2.14, 0.70 and 1.05, respectively, which are slightly greater than those of the isolated cylinder, reflecting the weak influence from the downstream cylinder.

On the other hand, the characteristics of the fluid forces of the downstream cylinder are significantly different from those of the upstream cylinder. The distribution tendencies of the drag and lift coefficients of the downstream cylinder are obviously irregular, which indicates that its vibration involves apparent random and unstable components. It is seen from Figure 4(e) that the oscillation of the drag coefficient roughly follows the third order mode, which is consistent with the vibration shape of displacement. Because of the shielding effect of the upstream cylinder, the drag of the downstream cylinder is much smaller than that of the upstream one. The maximum $C_{D\text{mean}}$ and $C_{D\text{std}}$ of the downstream cylinder is 0.72 and 0.33, respectively, and there is a moderate variation of the drag coefficient along its length. In addition, Figure 4(f) shows that the difference of the lift distribution between the two cylinders is not as significant as that of the drag. The oscillation of the lift of the downstream cylinder is mainly controlled by the sixth order mode, and the variations of $C_{L\text{std}}$ of two cylinders follow roughly the same trend. The amplitudes of the lift coefficient at the antinodes near both ends are greater than those near the middle of the downstream cylinder. The maximum $C_{L\text{std}}$ of the downstream cylinder is 1.00, which is close to that of the upstream cylinder.

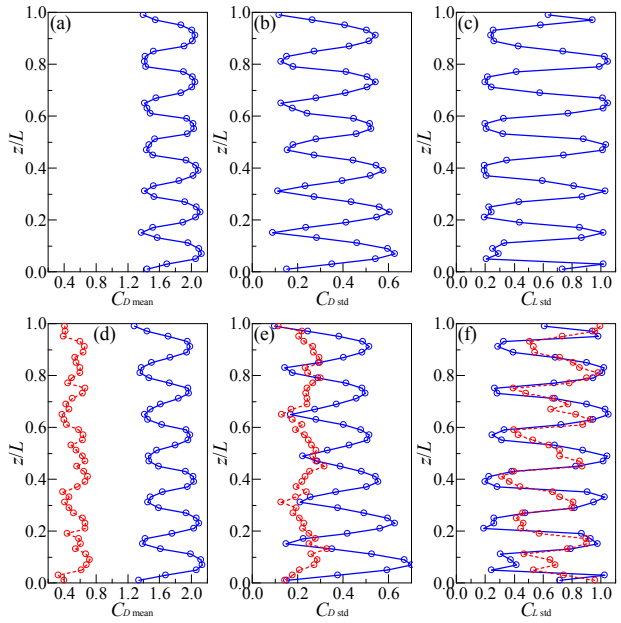

Figure 4. Fluid force coefficients for the isolated cylinder (a, b, c) and the tandem cylinders (d, e, f). Solid line: upstream cylinder; Dash line: downstream cylinder.

The vortex shedding pattern is investigated by the vorticity contours, where vorticity is defined as $\omega = \partial v/\partial x - \partial u/\partial y$. Figure 5 shows the vorticity contours in typical strips for the isolated cylinder and the tandem cylinders. The red and blue colors represent the positive and negative vorticity, respectively. The strips at z/L = 0.07 and 0.23 are located close to adjacent antinodes with large displacement, and the strips at z/L = 0.15 and 0.31 are located close to adjacent nodes with small displacement. This Figure shows, for the isolated cylinder, alternate vortex shedding from both sides of the cylinder in each vibration period, which coincides with the previously observed 2S vortex shedding mode. The vortex shedding patterns on two adjacent antinodes present anti-symmetric, which give rise to the opposite lift, and therefore leads to the opposite motion on two adjacent antinodes.

For tandem cylinders, the vortex shedding pattern of the upstream cylinder is similar to that of the isolated cylinder. Each vortex generated from the upstream cylinder completely sheds before it reaches the downstream cylinder, forming the classic 2S vortex shedding mode. This explains why the dynamic response of the upstream cylinder is similar to that of the isolated cylinder. In addition, the vortex shedding from the node of the upstream cylinder swings greater than that of the isolated cylinder, and its shedding distance is shorter. After shedding from the upstream cylinder, the vortex is crushed to the front surface of the downstream cylinder. It is also observed that the vortex shedding from the downstream cylinder is no longer periodic. The positive and negative vortex clusters form in turn far away from the downstream cylinder, which are not separated on both sides as the usual vortex street. The vortex shedding pattern of the

downstream cylinder is highly irregular, giving rise to irregular fluid forces on the downstream cylinder. As it is shown in Figure 4(f), the distribution of C_{Lstd} along the spanwise of the two tandem cylinders follow a similar trend. Hence it can be inferred that the lift force on the downstream cylinder is also affected by the alternate vortex shedding from the upstream cylinder.

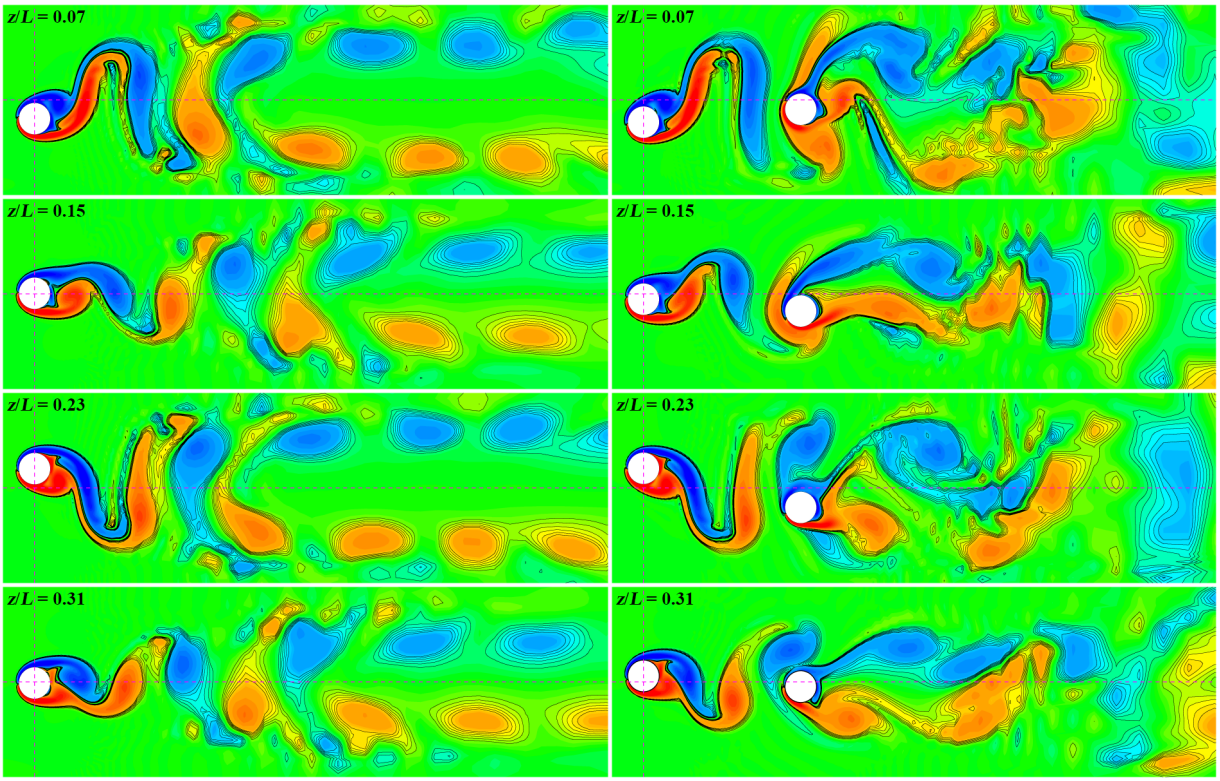

Figure 5. Vorticity contours for the isolated cylinder and the tandem cylinders.

Conclusions

VIV of two tandem flexible circular cylinders with a large aspect ratio of 3691 at a low Reynolds number of 200 is investigated numerically by a quasi 3D fluid structure coupling model based on strip theory. The numerical results show that when the centre-to-centre distance between the two tandem cylinders is 5*D*, the dynamic response of the upstream cylinder is very similar to that of the isolated cylinder, which indicates that the influence of the downstream cylinder is rather limited. The sixth mode vibration is excited on the upstream cylinder under the reduced velocity of 32.1. The distribution tendency of the displacement along the upstream cylinder is consistent with that of the drag, but is contrary to that of the lift. The periodical vortex street is observed for the upstream cylinder as well as the isolated cylinder. Because of the effect of wake interference, the response characteristic of the downstream cylinder is quite different from that of the upstream cylinder. The downstream cylinder behaves a significant irregular vibration, and its response is mainly controlled by the third order mode although multi-mode vibration is involved. The drag force on the downstream cylinder is much smaller than that of the upstream one due to the shielding effect. The vortex shedding pattern of the downstream cylinder is highly irregular, which is distinct to the regular 2S vortex shedding mode observed for the upstream cylinder.

Acknowledgments

This work is supported by the Natural Science Foundation of China (Grants 51409041, 51279029 and 51628901), and Liaoning Science and Technology Project (Grant 20141024).

References

[1] Assi, G. R. S., Bearman, P. W., Carmo, B. S., Meneghini, J. R., Sherwin, S. J., Willden, R. H. J. The role of wake stiffness on the wake-induced vibration of the downstream cylinder of a tandem pair. *J Fluid Mech*, 2013, 718: 210-245.

[2] Bearman, P. W. Circular cylinder wakes and vortex-induced vibrations. *J Fluid Struct*, 2011, 27(5-6): 648-658.

[3] Carmo, B. S., Meneghini, J. R., Sherwin, S. J. Secondary instabilities in the flow around two circular cylinders in tandem. *J Fluid Mech*, 2010, 644: 395-431.

[4] Lienhard, J. H. Synopsis of lift, drag, and vortex frequency data for rigid circular cylinders, Technical Extension Service, Washington State University, 1966.

[5] Tang, G.Q., Lu, L., Zhao, M, Liu, M.M., Zong Z. Phase jump and energy transfer of forced oscillating circular cylinder in uniform flow. *Proc IMechE Part M: Journal of Engineering for the Maritime Environment*, 2016, 1–15.

[6] Mittal, S. and V. Kumar. Flow-induced oscillations of two cylinders in tandem and staggered arrangements. *J Fluid Struct*, 2001, 15(5): 717-736.

[7] Schulz, K. W., Meling, T. S. Multi-strip numerical analysis for flexible riser response. *OMAE*, 2004, 379-384.

[8] Sumner, D. Two circular cylinders in cross-flow: A review. *J Fluid Struct*, 2010, 26(6): 849-899.

[9] Willden, R., Graham, J. Numerical prediction of VIV on long flexible circular cylinders. *J Fluid Struct*, 2001, 15(3): 659-669.

[10] Yamamoto, C., Meneghini, J., Saltara, F., Fregonesi, R., Ferrari Jr, J. Numerical simulations of vortex induced vibration on flexible cylinders. *J Fluid Struct*, 2004, 19(4): 467-489.

[11] Zhao, M. Flow induced vibration of two rigidly coupled circular cylinders in tandem and side-by-side arrangements at a low Reynolds number of 150. *Physics of Fluids*, 2013, 25(12): 123601.